Article:
Amara, Y., Wang, J.B. and Howe, D. (2005) Stator iron loss of tubular permanent-magnet machines. IEEE Transactions on Industry Applications, 41 (4). pp. 989-995. ISSN: 0093-9994

https://doi.org/10.1109/TIA.2005.851047

Stator Iron Loss of Tubular Permanent-Magnet Machines

Yacine Amara, Jiabin Wang, *Senior Member, IEEE*, and David Howe

***Abstract*—While methods of determining the iron loss in rotating permanent-magnet (PM) machines have been investigated extensively, the study of iron loss in linear machines is relatively poorly documented. This paper describes a simple analytical method to predict flux density waveforms in discrete regions of the laminated stator of a tubular PM machine, and employs an established iron loss model to determine the iron loss components, on both no load and on load. Analytical predictions are compared with the iron loss deduced from finite-element analyses for two tubular PM machine designs, and it is shown that if a machine has a relatively high electrical loading, the on-load iron loss can be significantly higher than the no-load value.**

***Index Terms*—Analytical model, iron loss, linear machines, permanent-magnet (PM) machines.**

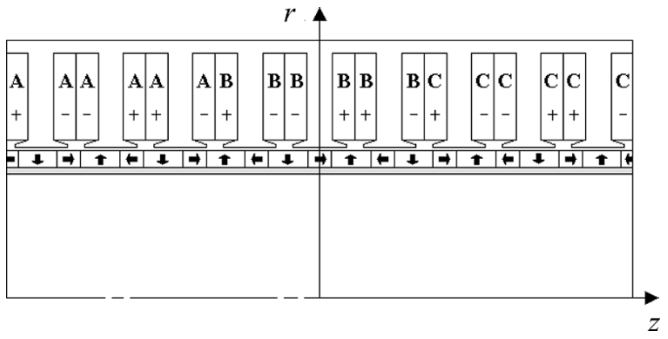

Fig. 1. Schematic of nine-slot tubular modular PM machine with quasi-Halbach magnetized armature.

I. Introduction

LINEAR electromagnetic machines, which can provide thrust force directly to a payload or generate electrical power from an applied thrust, are being developed for a wide spectrum of applications in market sectors as varied as manufacturing and household appliances [1]–[4]. They offer numerous advantages over rotary-to-linear motion systems. Of the various types and topologies of linear motor, tubular permanent-magnet (PM) machines are particularly attractive, since they have a high thrust force capability and no end-windings, and have zero net attractive force between the stator and armature.

However, while methods of determining the iron loss in rotating PM machines have been investigated extensively, the study of iron loss in linear machines is poorly documented. This paper uses a simple analytical model to predict flux density waveforms in discrete regions of the laminated stator of a tubular PM machine, and employs established analytical expressions to determine the iron loss components, on both no load and on load. Analytical predictions are compared with the iron loss deduced from finite-element (FE) analyses for two tubular PM machine designs, and it is shown that the on-load iron loss can be significantly higher than the no-load value.

The laminated stators of the two machines have the same topology, viz. nine teeth which carry a modular three-phase winding, in which the coils of each phase are accommodated in adjacent slots, as illustrated in Fig. 1, and the moving-magnet armature is quasi-Halbach magnetized, each pole comprising one radially magnetized ring magnet and one axially magnetized ring magnet. This machine topology has the advantages of high force capability, high efficiency, and low manufacturing cost, while the cogging force associated with the stator slotting can be very low. One machine was designed to produce a thrust force of 4 kN at a speed of 11 m/s (equivalent to a rated power of 44 kW) while the other was designed to produce a thrust force of 250 N at a speed of 6 m/s (equivalent to a rated power of 1.5 kW). In the high-power machine the PMs are mounted on a nonmagnetic tube, while in the low power machine they are mounted on a mild steel tube.

Paper IPCSD-05-015, presented at the 2004 Industry Applications Society Annual Meeting, Seattle, WA, October 3–7, and approved for publication in the IEEE TRANSACTIONS ON INDUSTRY APPLICATIONS by the Electric Machines Committee of the IEEE Industry Applications Society. Manuscript submitted for review August 20, 2004 and released for publication March 16, 2005.

The authors are with the Department of Electronic and Electrical Engineering, University of Sheffield, Sheffield, S1 3JD, U.K. (e-mail: j.b.wang@sheffield.ac.uk; d.howe@sheffield.ac.uk).

Digital Object Identifier 10.1109/TIA.2005.851047

II. Analytical Method

The analytical method of iron loss calculation employs analytical expressions reported in [5] for predicting the magnetic field distribution in the air gap due to the Halbach magnetized magnets and the three-phase stator winding, and, thereby, to deduce flux density waveforms in three discrete regions of the laminated stator core.

Fig. 2(a) shows the three regions, viz. tooth tip ①, tooth ②, and the back-iron ③. The iron loss density is calculated in each region using the experimentally verified iron loss density model defined in [6], [7], (1)–(3) being, respectively, the hysteresis loss component (neglecting minor hysteresis loops), the classical eddy-current loss component, and the excess eddy-current loss component

$$P_h = k_h f B_m^{\alpha} \tag{1}$$

$$P_c = \frac{2\pi\sigma d^2 f^2}{12\delta} \int_{2\pi} \left(\frac{dB}{d\theta_e}\right)^2 d\theta_e \tag{2}$$

$$P_e = \sqrt{2\pi} k_e f^{\frac{3}{2}} \int_{2\pi} \left|\frac{dB}{d\theta_e}\right|^{\frac{3}{2}} d\theta_e \tag{3}$$

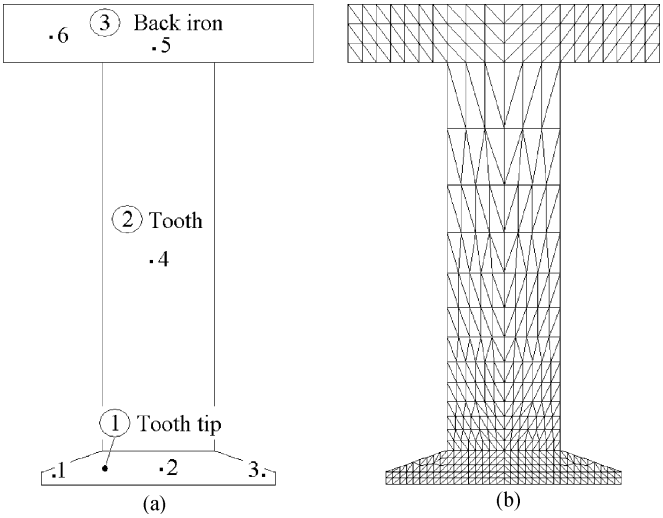

Fig. 2. Discretization of stator teeth pitch. (a) For analytical model. (b) For FE model (44-kW machine).

where f and B_m are the frequency and amplitude of the fundamental flux density; and σ, δ, and d are the electrical conductivity, the mass density, and the lamination thickness, respectively. k_h, α and k_e are experimentally determined loss coefficients, the values which were used for the calculations in this paper being given in the Appendix . The total iron loss is then given by

$$P_i = \sum_{m=1}^{M} (P_h + P_c + P_e)_m A_m 2\pi r_m \tag{4}$$

where A_m and r_m are the area of region m in the r–z plane and the radius of its mass center, respectively, and M is the total number of regions into which the stator is discretized, which is three in the analytical model. The same procedure is employed to estimate the iron loss both on n load and on load, and is equally applicable to the FE model, when M is the number of FEs into which the stator core is discretized [see Fig. 2(b)].

Analytical field solutions for the tubular PM machine are obtained by assuming that the ferromagnetic armature and stator cores are infinitely permeable [5]. In order to account for core saturation, however, a fictitious increase in air-gap length ΔG, given by

$$\Delta G = \frac{(F_{\rm ac} + F_{\rm sc})}{\frac{B_{\rm av}}{\mu_0}} \tag{5}$$

is introduced, where $F_{\rm ac}$ and $F_{\rm sc}$ are the magnetomotive force (MMF) drops in the armature and stator cores, respectively, and $B_{\rm av}$ is the average flux density at the stator bore, as described in [8]

A. No-Load Operation

1) Tooth Tip Region: The flux density in the tooth tip region is essentially alternating in the axial direction, and it experiences a rapid reversal in polarity as the PM armature moves past the teeth. Maximum flux density in the tooth tip region occurs after the axis of a tooth has coincided with a transition between magnet poles, as shown in Fig. 3. On open circuit, the maximum flux entering into the tooth tip region can be evaluated analytically from

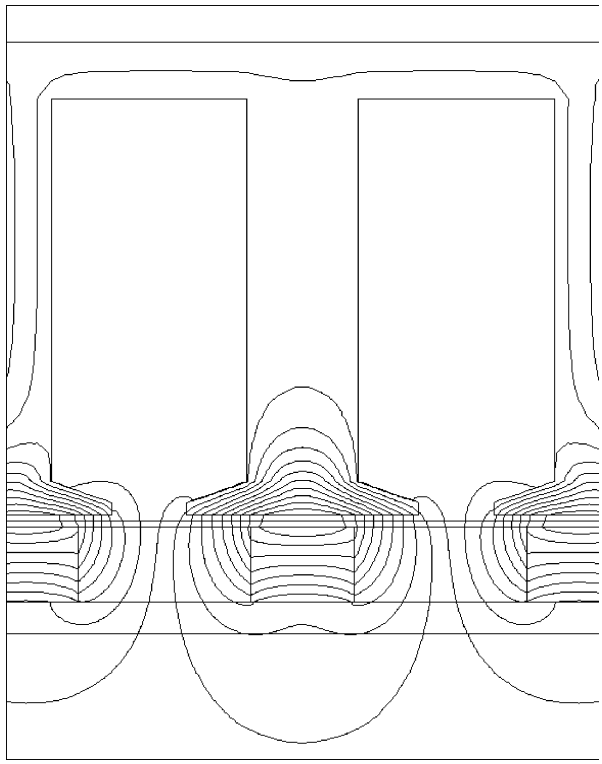

Fig. 3. No-load flux distribution when tooth axis coincides with interpole axis.

$$\Psi_{\max} = \frac{1}{2}\left(\int_{-\tau_{pt}/2}^{0} 2\pi R_s B_r dz - \int_{0}^{\tau_{pt}/2} 2\pi R_s B_r dz\right) \tag{6}$$

where B_r is determined using the expression given in [5], viz.

$$B_{Ir}(r,z) = \sum_{n=1,2,\ldots}^{\infty} [a_{In} BI_1(m_n r) + b_{In} BK_1(m_n r)] \sin(m_n z) \tag{7}$$

where $BI_0(\bullet)$, $BI_1(\bullet)$ are modified *Bessel* functions of the first kind; $BK_0(\bullet)$, $BK_1(\bullet)$ are modified *Bessel* functions of the second kind, of order 0 and 1, respectively; and a_{In} and b_{In} are given in [1]. The maximum flux density in the tooth tip region is, therefore,

$$B_{tp\max} = \frac{\Psi_{\max}}{\pi((R_s + h_t + t_{hh})^2 - R_s^2)} \tag{8}$$

where R_s is the stator bore radius, the other geometric parameters being defined in Fig. 4.

The transition time from flux of one polarity to the other is given by the following empirical equation:

$$t_a = \frac{\tau_{mz}\tau_p}{v\left(\tau_{mr} + \frac{2g}{\mu_r}\right)} \tag{9}$$

where g is the air-gap length, μ_r is the relative recoil permeability of the magnets, v is the linear speed of the armature, τ_{mr}

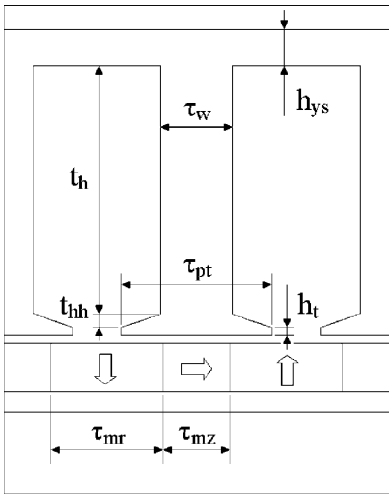

Fig. 4. Geometric parameters.

and τ_{mz} are, respectively, the axial lengths of the radially magnetized and axially magnetized ring magnets and τ_p is the pole pitch.

2) Tooth Region: The flux passing through the tooth can be obtained from the following integration:

$$\psi_t = \int_{\tau_{pt}/2}^{\tau_{pt}/2} 2\pi R_s B_r dz. \tag{10}$$

The flux is a maximum when the axis of a tooth coincides with the PM poles, as illustrated in Fig. 5, and is a minimum when the tooth axis coincides with a transition between magnet poles Fig. 3. The flux is predominantly radial, and flux density in the middle of tooth is given by

$$B_t = \frac{\psi_t}{2\pi\left(R_s + h_t + t_{hh} + \frac{th}{2}\right)\tau_w}. \tag{11}$$

3) Yoke Region: Similarly, the flux passing through the yoke can be obtained by the following integration:

$$\psi_y = \frac{1}{2}\int_{\tau_p/2}^{\tau_p/2} 2\pi R_s B_r dz. \tag{12}$$

However, the flux is now predominantly axial, and the flux density is given by

$$B_y = \frac{\psi_y}{\pi(R_e^2 - (R_e - h_{ys})^2)} \tag{13}$$

where R_e is the outer radius of the stator, and h_{ys} is the yoke thickness.

B. On-Load Operation

The on-load armature reaction field can also be derived analytically. The resultant field in the air gap is then obtained by superposition of the open circuit and the armature reaction fields. The flux density waveforms in the different regions of the stator and the on-load iron loss are then evaluated in the same way as under the no-load operation. By way of example, the current distribution in phase B of the slotted stator may be represented

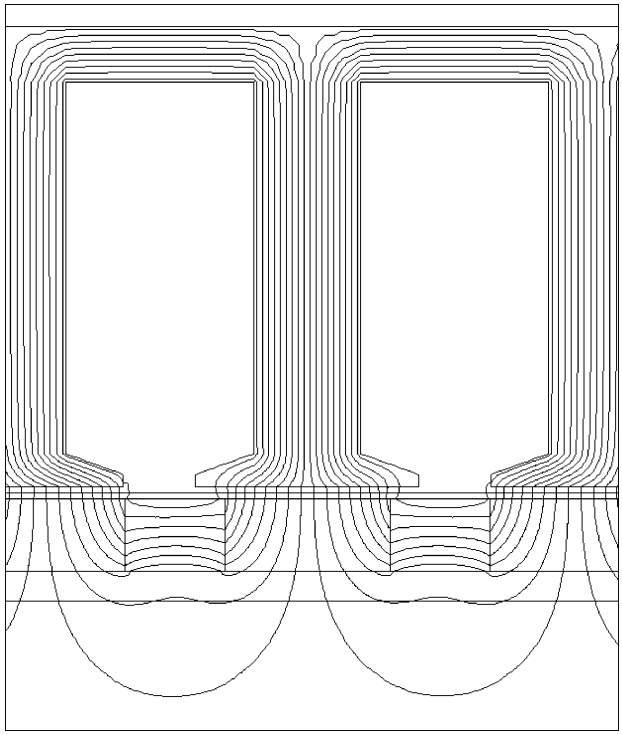

Fig. 5. No-load flux distribution when tooth axis coincides with pole axis.

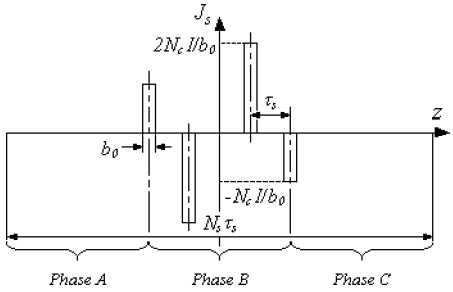

Fig. 6. Equivalent current sheet distribution in phase B.

using a current sheet model, as shown in Fig. 6, and can be expanded into a Fourier series of the following form:

$$J_{sb}(z) = \sum_{n=1}^{\infty} J_n \sin m_n z \tag{14}$$

where

$$J_n = \frac{2 \cdot N_c \cdot i}{\tau_p} \cdot K_{dcn} \cdot K_{pcn} \tag{15}$$

$$m_n = \frac{n \cdot 2 \cdot \pi}{N_s \cdot \tau_s} \tag{16}$$

$$K_{dcn} = \frac{\sin\left(\frac{m_n \cdot b_0}{2}\right)}{\frac{m_n \cdot b_0}{2}} \tag{17}$$

$$K_{pcn} = \frac{2 \cdot \tau_p}{N_s \cdot \tau_s} \cdot \left[2 \cdot \sin\left(\frac{n \cdot \pi}{N_s}\right) - \sin\left(\frac{3 \cdot n \cdot \pi}{N_s}\right)\right] \tag{18}$$

where N_c is the number of turns per coil, N_s is the number of slots over the modular pitch of ten poles, and i is the instantaneous value of current in phase B.

TABLE I
IRON LOSS COMPONENTS FOR HIGH-POWER MACHINE AT 11m/s (44 kW)

	Per unit iron loss							
	Hysteresis loss		Classical eddy current loss		Excess eddy current loss		Total iron loss	
	FE	Analytical	FE	Analytical	FE	Analytical	FE	Analytical
No-load	0.40	0.41	0.24	0.24	0.36	0.34	1.00	0.99
Rated load	0.94	0.98	0.54	0.56	0.66	0.63	2.14	2.17

TABLE II
IRON LOSS COMPONENTS FOR LOW-POWER MACHINE AT 6 m/s (1.5 kW)

	Per unit iron loss							
	Hysteresis loss		Classical eddy current loss		Excess eddy current loss		Total iron loss	
	FE	Analytical	FE	Analytical	FE	Analytical	FE	Analytical
No-load	0.39	0.39	0.27	0.27	0.34	0.33	1.00	0.99
Rated load	0.45	0.47	0.30	0.30	0.37	0.36	1.12	1.13

In order to establish an analytical solution for the armature reaction field, the axial length of the machine is assumed to be infinite, and the stator core is assumed to be infinitely permeable. Since the field is axially symmetrical, the vector magnetic potential A only has the component A_θ, which is independent of θ. The field equation, in terms of A_θ, is then given by

$$\frac{\partial}{\partial z}\left(\frac{1}{r}\frac{\partial}{\partial z}(rA_\theta)\right)+\frac{\partial}{\partial r}\left(\frac{1}{r}\frac{\partial}{\partial r}(rA_\theta)\right)=0. \quad (19)$$

The boundary conditions to be satisfied by (19) are given by

$$\begin{cases} B_z|_{r=R_0}=0, & \text{for a nonmagnetic support tube} \\ B_r|_{r=0}=0, & \text{for a magnetic support tube} \end{cases}$$
$$H_z|_{r=R_s}=J_s \quad (20)$$

where R_0 is the outer radius of the mild steel support tube of the smaller machine. A field solution is obtained by solving (19) subject to the boundary conditions of (20), By way of example, with a nonmagnetic support tube, flux density components are given by

$$B_r=-\sum_{n=1}^{\infty}[A_n\cdot BI_1(m_n\cdot r)\cdot m_n\cdot\cos(m_n\cdot z)]$$
$$B_z=\sum_{n=1}^{\infty}[A_n\cdot BI_0(m_n\cdot r)\cdot m_n\cdot\sin(m_n\cdot z)] \quad (21)$$

where

$$A_n=\frac{J_n\cdot\mu_0}{BI_0(m_n\cdot R_s)\cdot m_n}. \quad (22)$$

The flux density components due to phases *A* and *C* can similarly be obtained, by shifting the axial displacement by $\pm 2\tau_p/3$. The resultant armature field reaction is then obtained by summing the armature reaction fields of the three phases.

III. VALIDATION

FE analysis has been used to assess the validity of the developed analytical method for predicting the stator iron loss in tubular PM machines. It has been applied to two machines with different power ratings. The flux density waveforms in the stator core are calculated by time-stepped FE analysis, and the stator iron loss is evaluated using (1) to (4).

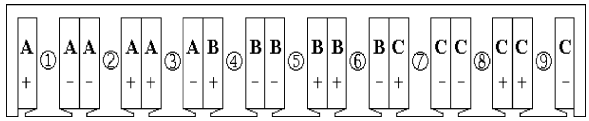

Fig. 7. Different groups of teeth.

Tables I and II compare the iron loss components for the two machines operating on no-load and at rated-load and at rated speed. For each machine, the losses are normalized to the total no-load value obtained by FE analysis. It should be noted that the on-load iron loss in the high-power machine is significantly higher than the no-load value. This is due to the fact that its stator is water cooled, and, hence, has a relatively high electric loading. The associated armature reaction field is, therefore, much stronger, and results in a higher saturation level, significant flux harmonics, and, consequently, a greater iron loss.

It should be noted that on no load the loss in each tooth of the stator is the same. However, under load conditions, the flux density waveforms which result from the combined effect of the open-circuit and armature reaction fields are different in each tooth of a phase module. Consequently, the iron loss in three groups of teeth, viz., [①, ④, ⑦], [②, ⑤, ⑧], and [③, ⑥, ⑨], as defined in Fig. 7, are different. The analytical method is, therefore, applied to one tooth in each group, and the total loss is the sum of the loss in three groups of teeth

$$P_t=3(P_1+P_2+P_3) \quad (23)$$

where P_1, P_2, and P_3 are the iron losses in teeth 1, 2, and 3, respectively.

Fig. 2(a) shows the various points in the stator core at which analytically derived flux density waveforms have been compared with that deduced from FE analysis for the larger machine under no-load and rated load operation. Figs. 8–10 compare the FE and analytical flux density waveforms on no load, in the tooth tip, tooth body, and back-iron regions, respectively. Similar comparisons for the rated load conditions are given in Figs. 11–13 for tooth ③. As will be seen, the FE and analytically predicted flux density waveforms in the tooth body and back-iron regions agree reasonably well both on no load and at rated load. The flux density waveforms in the tooth tip region

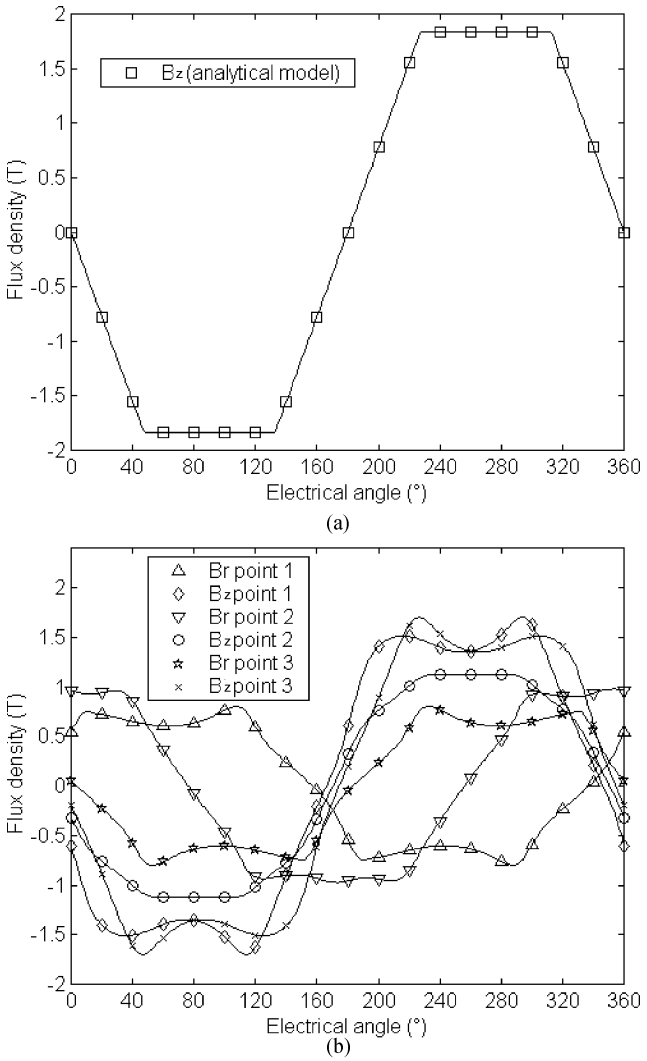

Fig. 8. Comparison of no-load flux density waveforms in tooth tip. (a) Analytical (b) FE.

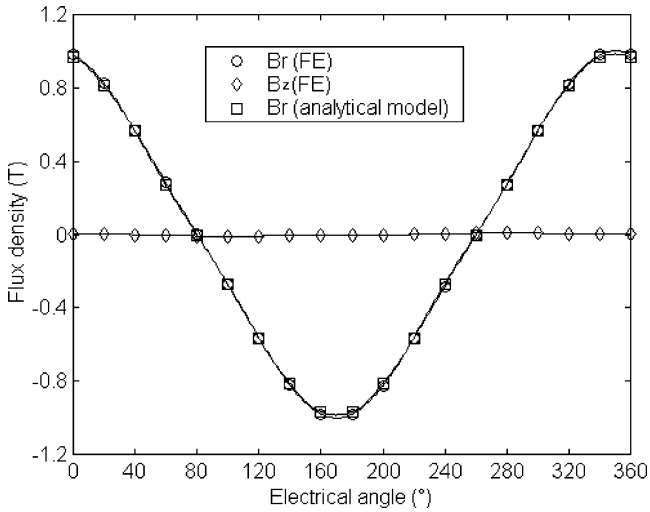

Fig. 9. Comparison of no-load flux density waveforms at point 4 in tooth.

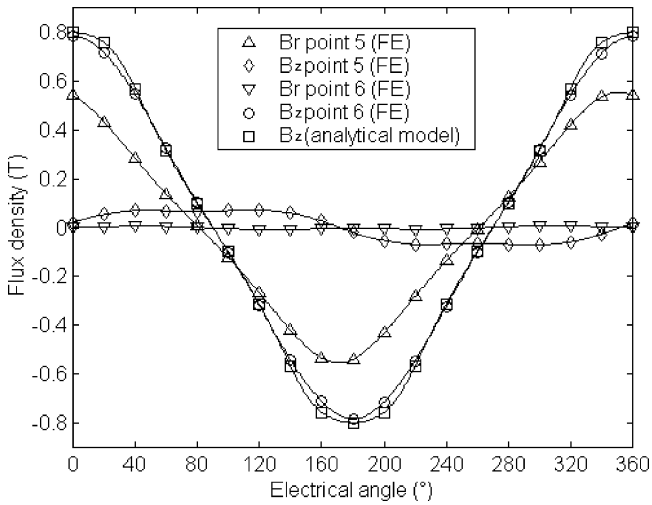

Fig. 10. Comparison of no-load flux density waveforms in back-iron.

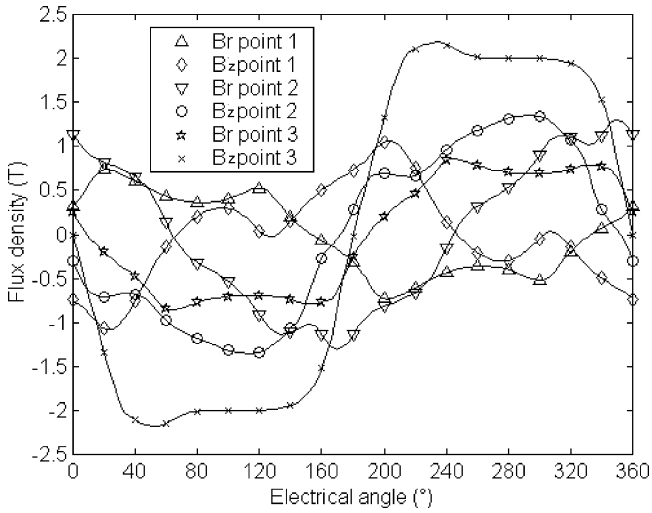

Fig. 11. Full-load flux density waveforms in tooth tip.

are, however, much more complex, and vary with axial position. Thus, the analytically predicated flux density waveforms can only approximate the actual waveforms.

Despite the fact that the FE and analytically predicted flux density waveforms do not compare very well in the tooth tip regions, and the fact that the analytically calculated iron loss is determined only from the dominant single component of flux density in each of the three regions, while the FE calculated value accounts for the loss due to each orthogonal flux density component in each element, the total iron loss predicted by the two methods is in good agreement.

By way of example, Fig. 14 compares the variation of the analytically and FE predicted iron loss of the larger machine on no load and at rated load as a function of the armature speed. As will be evident, the iron loss predicted by the two methods agrees well. Fig. 15 shows a similar comparison for the smaller machine. Again, good agreement is obtained between the analytical and FE predictions.

It should be noted that the iron loss in the tooth tips is quite similar under the full-load and on-load conditions. This is due to the fact that the armature reaction field tends to increase the flux density on one side of a tooth tip and decrease it on the other side. Thus, the total iron loss does not change significantly.

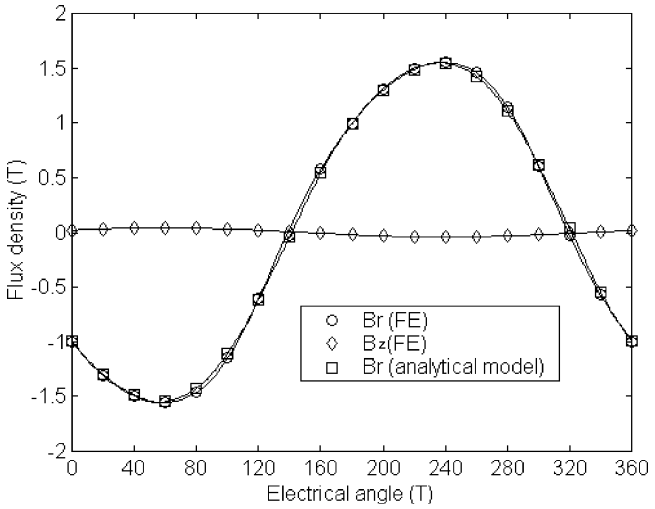

Fig. 12. Comparison of full-load flux density waveforms at point 4 in tooth.

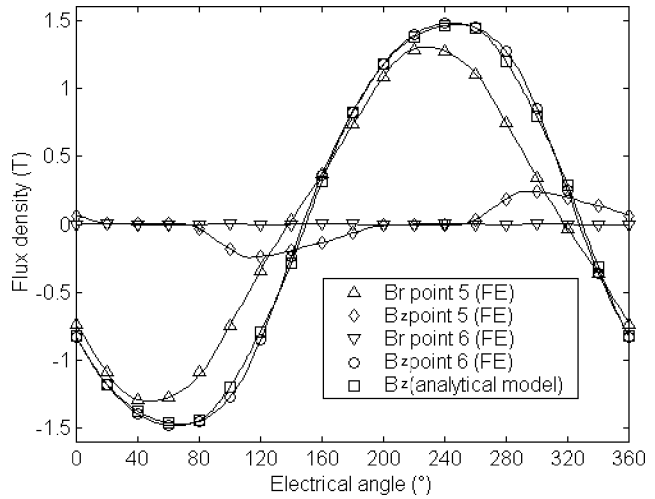

Fig. 13. Comparison of full-load flux density waveforms in back-iron.

Experimental validation of the predictions is extremely challenging, since most linear machines operate in reciprocating systems, and are, therefore, constantly being accelerated and decelerated. Furthermore, in practice, the actual core loss will also be sensitive to the lamination stack pressure and mechanical stress, and will be affected by the presence of burrs on the laminations, effects which are difficult, if not impossible to model. Nevertheless, it has been shown [6], [7] that iron loss prediction by time-stepped FE analysis, using experimentally determined iron loss coefficients for the particular grade of lamination material, and based on an experimentally validated iron loss model is extremely accurate, and, therefore, may provide adequate validation of the proposed analytical method. However, further experimental work is still necessary in order to ultimately validate the proposed method.

It should also be noted that due to the MMF space harmonics of the stator winding and the slotting effect of the stator core, eddy current losses will also be induced in both the magnets and supporting tube (if they are electrically conductive). The techniques for predicting these losses have been reported in [10] and [11].

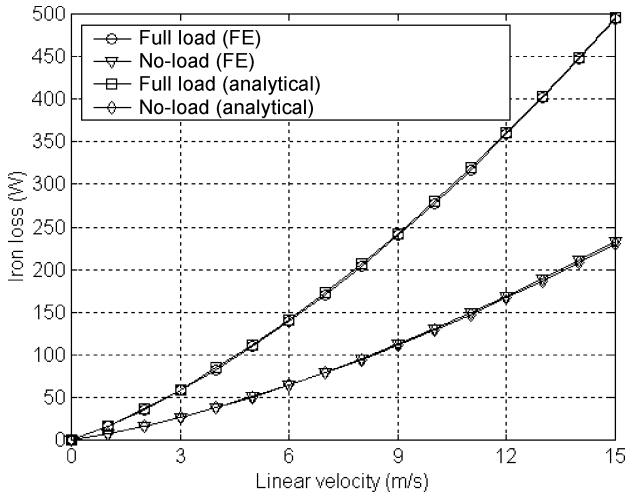

Fig. 14. Variation of iron loss with speed (44-kW machine).

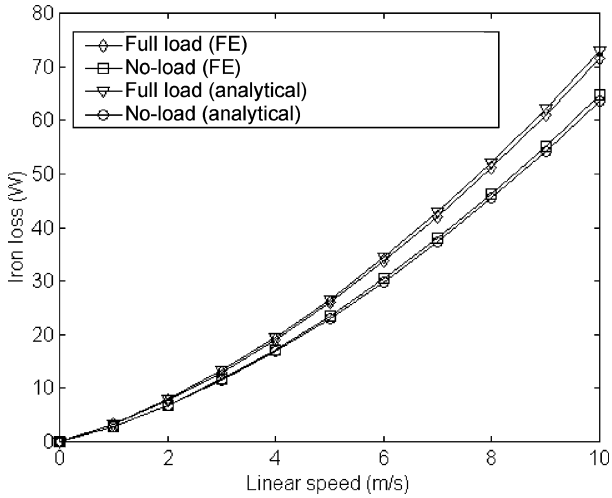

Fig. 15. Variation of iron loss with speed (1.5-kW machine).

TABLE III
MATERIAL CHARACTERISTICS (TRANSIL300)

Name	Value
Lamination density δ (kg / m^3)	7650
Lamination thickness d (mm)	0.35
Conductivity σ (Ω^{-1} m^{-1})	1.33 x 10^6
Loss constant α	2.45
Loss constant k_h	15.5 x 10^{-3}
Loss constant k_e	0.1 x 10^{-3}

IV. CONCLUSION

A relatively simple analytical method to predict the stator iron loss in tubular linear PM synchronous machines has been described. Its utility has been demonstrated on two linear machines under both no-load and full-load conditions. It has been shown that, despite the simplicity of the analytical model, the predicted iron loss is in excellent agreement with that deduced from FE analysis. The analytical tool should, therefore, be useful for comparative design studies, and aid design optimization.

APPENDIX

See Table III.

REFERENCES

[1] J. F. Eastham, "Novel synchronous machines: Linear and disc," *Proc. Inst. Elect. Eng.*, pt. B, vol. 137, pp. 49–58, 1990.

[2] E. Masada, "Linear drives for industrial applications in Japan — History, existing state and future prospect," in *Proc. LDIA'95*, 1995, pp. 9–12.

[3] W. R. Cawthorne, P. Famouri, J. Chen, N. N. Clarke, T. I. McDaniel, R. J. Atkinson, S. Nandkumar, C. M. Atkinson, and S. Petreanu, "Development of a linear alternator-engine for hybrid electric vehicle applications," *IEEE Trans. Veh. Technol.*, vol. 48, no. 6, pp. 1797–1802, Nov. 1999.

[4] K. Park, E. P. Hong, and K. H. Lee, "Development of a linear motor for compressors of household refrigerators," in *Proc. LDIA'01*, 2001, pp. 283–286.

[5] J. Wang, D. Howe, and M. Inoue, "Magnetic field distribution of quasi-Halbach magnetised cylinder for tubular permanent magnet machines," in *Proc. LDIA'03*, 2003, pp. 481–484.

[6] G. Bertotti, A. Boglietti, M. Chiampi, D. Chiarabaglio, F. Fiorillo, and M. Lazzari, "An improved estimation of iron losses in electrical machines," *IEEE Trans. Magn.*, vol. 27, pp. 5007–5009, 1991.

[7] K. Atallah and D. Howe, "The calculation of iron losses in brushless permanent magnet dc motors," *J. Magn. Magn. Mater.*, vol. 133, pp. 578–582, 1998.

[8] J. Wang, G. W. Jewell, and D. Howe, "Design optimization and comparison of tubular permanent magnet machine topologies," *Proc. IEE—Elect. Power Appl.*, vol. 148, no. 5, pp. 456–464, 2001.

[9] ——, "A general framework for the analysis and design of tubular linear permanent magnet machines," *IEEE Trans. Magn.*, vol. 35, no. 3, pp. 1986–2000, May 1999.

[10] Y. Amara, J. Wang, and D. Howe, "Eddy current loss in tubular modular permanent magnet machines," in *Proc. ICEM'04)*, Cracow, Poland, 2004, Paper 193, pp. –.

[11] ——, "Analytical prediction of eddy current loss in modular tubular permanent magnet machines," *IEEE Trans. Energy Convers.*, to be published.

Yacine Amara was born in Algiers, Algeria, in 1975. He received the B.Eng. degree in electrical engineering from the Ecole Nationale Polytechnique of Algiers, Algiers, Algeria, in 1997, the DEA degree in electrical engineering from the University of Pierre et Marie Curie (Paris VI), Paris, France, in 1998, and the Ph.D. degree from the University of Paris Sud XI, Orsay, France, in 2001.

From 1998 to 2001, he was a Ph.D. student in the Laboratoire d'Electricité Signaux et Robotique (LESiR), Ecole Normale Supérieure de Cachan, France. From 2001 to 2002, he was an Assistant Professor in the Department of Physique at the University of Paris Sud XI. He is currently a Research Associate at the University of Sheffield, Sheffield, U.K. His research interests include the design, modeling, and control of rotating and linear permanent-magnet machines for automotive applications.

Jiabin Wang (SM'03) was born in Jiangsu Province, China, in 1958. He received the B.Eng. and M.Eng. degrees from Jiangsu University of Science and Technology, Zhengjiang, China, in 1982 and 1986, respectively, and the Ph.D. degree from the University of East London, London, U.K., in 1996, all in electrical and electronic engineering.

Currently, he is a Senior Lecturer at the University of Sheffield, Sheffield, U.K. From 1986 to 1991, he was with the Department of Electrical Engineering at Jiangsu University of Science and Technology, where he was appointed a Lecturer in 1987 and an Associate Professor in 1990. He was a Postdoctoral Research Associate at the University of Sheffield from 1996 to 1997 and a Senior Lecturer at the University of East London from 1998 to 2001. His research interests range from motion control to electromagnetic devices and their associated drives.

David Howe received the B.Tech. and M.Sc. degrees from the University of Bradford, Bradford, U.K., in 1966 and 1967, respectively, and the Ph.D. degree from the University of Southampton, Southampton, U.K., in 1974, all in electrical power engineering.

He has held academic posts at Brunel and Southampton Universities, and spent a period in industry with NEI Parsons Ltd., working on electromagnetic problems related to turbogenerators. He is currently a Professor of Electrical Engineering at the University of Sheffield, Sheffield, U.K., where he heads the Electrical Machines and Drives Research Group. His research activities span all facets of controlled electrical drive systems, with particular emphasis on permanent-magnet excited machines.

Prof. Howe is a Chartered Engineer in the U.K., and a Fellow of the Institution of Electrical Engineers, U.K., and the Royal Academy of Engineering.